Article

Not peer-reviewed version

Chorda Dorsalis System as a Paragon for Locally Actuated Compliant Bending Beams to Improve the Performance of TEE Probes

Mostafa Sayahkarajy *, Hartmut Witte *, A. Athif M. Faudzi

Posted Date: 14 February 2024

doi: 10.20944/preprints202402.0787.v1

Keywords: soft mechanisms; biomimetic development; medical device; automation of transesophageal echocardiography; TEE

Article

Chorda Dorsalis System as a Paragon for Locally Actuated Compliant Bending Beams to Improve the Performance of TEE Probes

Mostafa Sayahkarajy [1,*], Hartmut Witte [1,*] and A. Athif M. Faudzi [2]

[1] Fachgebiet Biomechatronik, Technische Universität Ilmenau, 98693 Ilmenau, Germany; mostafa.sayahkarajy@tu-ilmenau.de (M.S.); hartmut.witte@tu-ilmenau.de (H.W.)
[2] Centre for Artificial Intelligence and Robotics, Universiti Teknologi Malaysia, Kuala Lumpur 54100 Malaysia; athif@utm.my
* Correspondence: mostafa.sayahkarajy@tu-ilmenau.de (M.S.); hartmut.witte@tu-ilmenau.de (H.W.)

Abstract: Continuum robots play the role of end-effector in various surgical robots and endoscopic devices. The robots may be categorized as rigid or soft continuum robots (SCRs). While the SCRs have proven advantages such as safety and compliance, more research and development are required to enhance their capability for specific medical scenarios. This research aims at designing a soft robot considering concepts of geometric and kinematic similarities. The chosen application is a semi-invasive medical application known as Transesophageal Echocardiography (TEE), but the methodology can be implemented in other similar applications. Since established rigid carrier construction make use of principles we find as well embodied in vertebral spines, the paragon for soft robot solution can be the phylogenetic precursor of the spine, the *Chorda dorsalis*. The feasibility of fabrication of a soft endoscopic device derived from that paragon within a robotics laboratory was shown empirically by producing a three-segment pneumatic SCR. The kinematic model was proposed based on the method of transformation matrices, and an algorithm based on a self-organizing map (SOM) was proposed and applied to realize kinematic similarity. The simulation results indicate that the algorithm acting as an open-loop controller forces the soft robot tip to follow the desired path which in this case is the path of the rigid probe. It is concluded that the solution provides a soft robot that can surrogate and succeed the traditional rigid counterpart owing to size, workspace, and kinematics.

Keywords: soft mechanisms; biomimetic development; medical device; automation of transesophageal echocardiography

1. Introduction

Beneath other factors, available materials and technologies determine technical design. Natural inorganic rigid materials ("stone") and organic semi-rigid to compliant materials (plant materials like wood and animal materials like tendons) via technology were supplemented by more moldable ("opera cementum" – concrete) and more malleable ductile instead of brittle inorganics (metals), and as well bio-analogue and bio-inspired organics (rubber and other polymers). Today desired combinations of rigidity and strength can be achieved using a variety of compound materials.

Learning about energy efficiency and adaptability of organisms, "soft construction" gains growing interest. "Soft" here mostly is used in a wrong way, it usually resembles "compliant". "Soft" and "hard" and "compliant" and "rigid" roughly correlate but address different properties. The components of compliance "elasticity" (springiness) and "damping" are of special interest what concerns optimization of energy management in movement processes and their mechanical stability.

In industrial manipulation robotics, compliance is increasingly used to protect people in human-robot cooperation to minimize energy transfer and contact force exchange [1]. Such robots can rely on flexibility due to the slenderness of their links or rotational spring effects implemented in the joints. "Soft robotics" of motion machines, on the other hand, has so far found little acceptance in commercial practice. The main obstacles are doubts about the precision of production, but also the

 doi:10.20944/preprints202402.0787.v1

precision and reproducibility of movements. With this article, we would like to contribute a bionic approach to the utilization of soft robotics principles in products. To this end, we have focused on a particularly critical field of application for biomechatronics and biomedical engineering, in addition to our biorobotics developments since 2002 which are not to be addressed here.

Reproducible precision plays a central role in biomedical engineering. Therefore, safety-critical mechanisms today always are rigid-body systems; compliant elements only play a role in defined subtasks such as targeted energy storage and release (*e.g.*, as springs in injection pens), and usually are realized by "classic" metals, polymers, and compounds. Applications of elastic energy storage in prostheses, orthoses and exoskeletons are biosimilar and closely related to locomotion robotics, whereby new control strategies play a central role to mirror the precision of macroscopic human body movements. This has in combination with spring elements already been realized in products for "gross motor skills" (cm), but developments for "fine motor skills" (mm to sub-mm, e.g., manipulation) still present major difficulties.

A technology bridge can offer a view of actuators that can handle low loads and prioritize the representation of displacement values instead of providing larger load-bearing forces and energy transfers. A typical example of this is inspection tasks. We have already realized a bionic implementation for these in a technical environment with the Rat-Nic lightweight robot (m = 1.1 kg) [2]. In the more challenging task of how established biomedical engineering systems can be improved biomimetically with compliant mechanisms, endoscopic systems are currently the group of our study objects under consideration. Continuum robots (which are not really using continua) inspired by creatures like snakes or elephant trunks have the ability to pass through narrow orifices and access points, e.g., inside the human body, either for observation purposes, e.g., via endoscopy, or operations, or in surgical robots [3,4]. Conventional robots and mechanisms contain rigid components inherent in industrial applications and lack the flexibility and thus adaptability of organisms [5]. The non-compliant material of rigid mechanisms introduces high-risk hazards in human-machine interaction by applying unwantedly high mechanical forces on the tissue. This hazard can be seriously critical in the case of invasive or semi-invasive medical applications, where an end effector is manipulated inside the patients' body. The current technology of rigid mechanisms employs joints with bearings, gears, and different types of coupling. The metal parts make the system heavy and provoke additional problems due to friction and rigidity.

For the meso size range of medical devices like endoscopic devices, we see the opportunity for an improvement in the performance by an approach based on biomimetics. We tested whether a biomimetic approach may improve performance and decrease security risks. For this test, a demonstrator system was developed.

Application Case

The technical part of biomimetics must be directed to a defined application case. We chose the improvement of the Transesophageal Echocardiography (TEE) probe. TEE is a cardiac imaging modality to get cross-sectional images of the patient's heart based on backscattered ultrasound (US) waves [6]. Measurements are taken from the direct neighborhood of the heart, thus avoiding the masking effects of the rips in external echocardiography and allowing complete 3D reconstruction of the organ. A conventional TEE probe carries an ultrasound transducer mounted at the tip of an endoscope, which is manually operated by a physician. The TEE process underlies significant risks such as human errors, exposure to ionizing radiation, and multitasking complexity, leading to injuries. While medical devices are fabricated with the highest standards, their possible applications are restricted by technological limitations. Further improvements in terms of control, safety, and workload of the operator must be found beyond the established design and fabrication methods of commercialized industrial systems.

The traditional endoscopic probes used in invasive or semi-invasive modalities such as TEE and gastroenterology use an insertion tube to convey the sensor into the patient's body. The concept then is to orientate the rigid "head" of the endoscope by bending the connection ("neck") to the following semi-rigid "body" in 2 DoF in such a way, that driven by axial forces ("propulsion") the head glides

 doi:10.20944/preprints202402.0787.v1

through the anatomically preformed cavities with minimized contact, and if it occurs, minimized contact forces. The TEE probe can be explained as a wire-driven linkage of rigid parts, providing mechanical bending to right-left and up-down directions. TEE tube diameter (approximately 1 cm) is not convenient to pass through the human esophagus. Although the insertion part is termed flexible, it is rather stiff, and when it is bent during the operation, the bent section is not compliant. The relative motion between the head and tail may be described around one bending axis defined by the overlay of the two bending components. A critical hazard in the TEE operation is that the physician fails to straighten the probe before removing the probe from the esophagus. Manipulation of the probe in an incorrect position in the patient's body exerts high forces which can rupture the soft tissues. In addition to hazards and difficulties threatening the patients, the traditional probes have limitations for the users, i.e., the sonographers, in terms of manipulation and ergonomics. It is difficult and needs intense training to manipulate the probe, especially with one single hand. Turning the knobs needs moderate finger force, and tip position control is not easy. Assurance of the quality of the application process counts on the training of the user and their skill. Researchers thus propose robot-assisted solutions for ultrasonic examinations [7,8].

Some robots have been developed to assist TEE [9–11] that are actually master-slave holders, manipulating the probe handle for the remote user. In [11] it is discussed that such holders have no control over the subsection of the probe between tip and holder, and an additional support arm was suggested to alleviate the problem. Such rigid robots keep the probe without any change and add further complexities to it, while a soft robot may serve as a replacement for the probe. Soft robotics, employing the concept of biology for engineering (Bio4Eng [12]), mimics the soft body of live creatures or replicates biological systems [13,14]. Soft actuators, powered by pneumatic or fluidic pressures [15] are concurrently developed to replicate biological muscles [4]. They are, essentially, of low weight and do not need bearings, gears, and metal parts, and thus avoid the above-described problems. Applicability of existing control equipment like pneumatic valves is an advantage of soft robots that work with industrial level pressures, though research is ongoing to develop fully soft pneumatic logic systems [16]. Soft robotics is seen as a new way to redesign future generations of current medical systems, attracting investors and companies for product commercialization. The vision is not limited only to the replication of conventional systems and competing with them but tackling a set of problems that existing technologies have not been able to solve. In this perspective, biomedical applications of soft robotics embrace rehabilitation, tissue engineering, soft biological cell biology, flexible surgical manipulators, etc. [17–19]. In particular, continuum robots that play the main roles in many robotic surgery and US scenarios can be supplemented by soft robots.

Nevertheless, more investigations are required to explore the feasibility and applicability of soft robots for a defined intended medical application. Depending on the specific medical application, different sizes and ranges of motion are required, while soft robots are commonly taken into consideration for basic mechanical performances in locomotion and manipulation. Additionally, the introduction of a new soft robot to the medical community should not impose extensive training. Users who have gained comprehensive training and experience with rigid medical setups may not show dexterity with a new robot with a different actuation system or DoFs. The situation is comparable to the introduction phase of minimally invasive surgery. As an example, this article aims to propose a conceptual soft robotic solution for the TEE application and to develop the model and design for a demonstrator. One technical approach is to employ soft pneumatic actuators (SPAs) to play the role of current TEE probes. The main design considerations include the size or scale, workspace, and path following the robot tip where the US sensor is placed. The design, fabrication, and model are presented, and a novel self-organizing map (SOM) -based algorithm is proposed for controlling the robot.

Preprints.org (www.preprints.org) | NOT PEER-REVIEWED | Posted: 14 February 2024 doi:10.20944/preprints202402.0787.v1

2. Materials and Methods

2.1. Existing Reference Systems

The TEE probe mechanism technically can be described as serially connected rigid links driven by a cable passed through the links. The cable goes around a pulley and is driven manually with rotation knobs known as "big" and "small" wheels. Figure 1 shows actual probes used in hospital for adult patients. The probes are of different types, namely T6210, X7-2t, and IPX-1 from Philips®. All probes possess the same mechanical dimensions and exhibit similar bending when the wheels were rotated. This rotation causes the straight part at the tip to be located in desired poses. The fact that only the distal section of the probe is inserted in the patient body, as in Figure 1 (b), encouraging us to think of a soft robot of as a replacement. The proximal part of the tube, from the active part to the handle, is mechanically passive. The big wheel provides the anteflexion-retroflection, and the small wheel provides lateral bending.

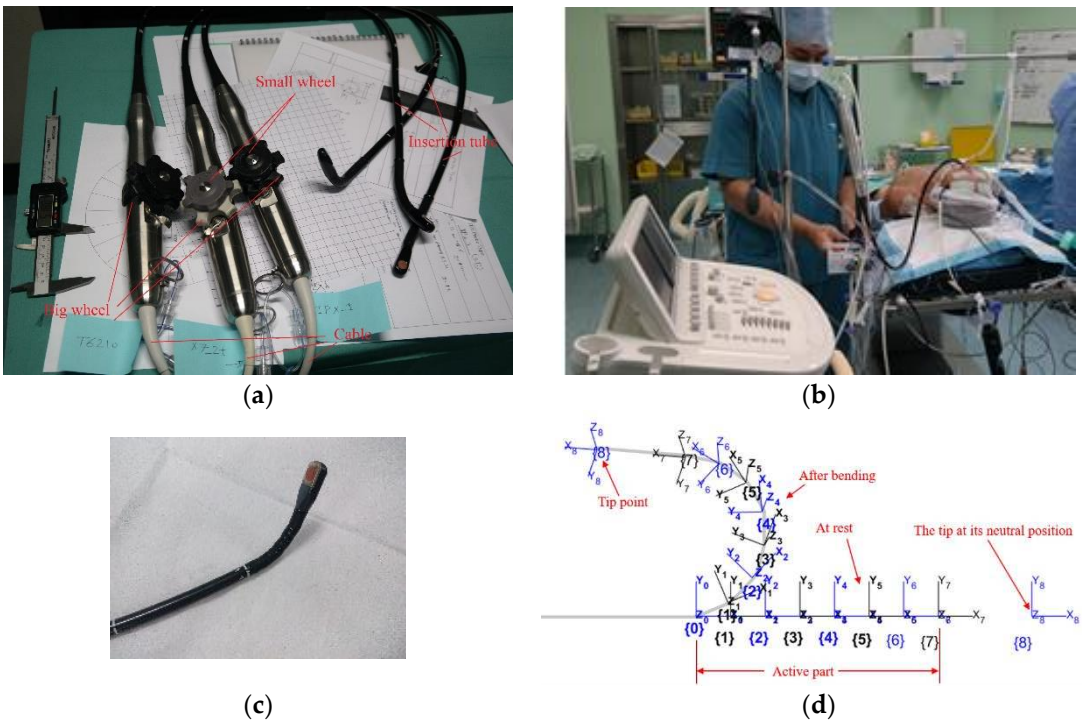

Figure 1. The conventional system: (a) Philips® TEE probes used for adult patients, (b) Example of application in surgery, (c) The distal section, and (d) Linkage coordinate systems.

The probe kinematic model can be constructed of two parts, where the first part maps the inputs which is the rotation of the wheels of the TEE probe [11] to the probe states (bending and flexing angles). The same pattern is used for the soft probe where the inputs (contraction of the McKibben actuators) are mapped to the segmental bending and rotations. The second part of the kinematic model relates the states to the tip position. The state-output relations can be used for workspace evaluation for the different probes. For the TEE probe, a model is considered to consist of some serially connected links as in Figure 1 (d), where $X_8Y_8Z_8$ is located at the tip and Z_8 is normal to the sensor. Each link rotates around the Z-axis of the previous link in ante flex-retroflex, and around the relevant Y-axis in the lateral bending. Mathematically, each coordinate i is obtained by rotating the previous system of angle θ_{zi} around Z_{i-1}, followed by a translation l_i (=length of the link) along the new coordinate, followed by a rotation θ_{yi} around the new Y-axis002E

$$T_i = Rotz(\theta_{zi})Trans(l_i,0,0)Roty(\theta_{yi}) \quad (1)$$

 doi:10.20944/preprints202402.0787.v1

Ignoring friction and extensibility of the cables, it can be supposed that the links have similar conditions, and so the links show equal rotations, i.e., $\theta_{zi} = \theta_z$, $\theta_{yi} = \theta_y$. A homogeneous transformation matrix, *H*, relates the tip position in frame 8 to its position vector in frame 0 as

$$H = T_1 T_2 T_3 ... T_8 \quad , \quad \vec{P}^0_{Tip} = H\vec{P}^8_{Tip} \tag{2}$$

The reachable work space is defined as the set of tip point positions $\vec{P}^0_{Tip}$ that can be reached by some choice of state vector, $\vec{q}_R$, within the set of admissible states Q^{rigid}

$$W^{rigid} = \left\{ \vec{P}^0_{Tip} \middle| \vec{q}_R \in Q^{rigid} \right\} \subset \mathbb{R}^3 \tag{3}$$

Where the state vector is described by constant curvature rule as $\vec{q}_R = \left[\theta_z, \theta_y \right]^T$; and Q^{rigid} can be represented by the range of the angles obtained from measurements as

$$Q^{rigid} = \left\{ \vec{q} \middle| 0 < \theta_z < 18^o, 0 < \theta_y < 7^o \right\} \tag{4}$$

Then, using (2) and (4) in (3), a set of reachable points is obtained, denoted as W^{rigid}. The next steps were to design and fabricate a soft robot, and to propose a method to match the input-outputs kinematics of the soft robot to that of the conventional system as described in the following subsections.

2.2. Biomimetic Concept

From a technical perspective, present endoscopes are bending beams with a rather stiff "body", and a "neck" with under-actuated rotatory DoFs (Degrees of Freedom) around two orthogonal bending axes each. This principle biologically roughly mirrors a motion segment [20] of a vertebral column (without the rotatory DoF around the longitudinal axis, which leads to torsion of the spine), or a mechanically coupled (not independently movable) series of motion segments. The desirable extreme to optimize the versatility and adaptability of endoscope to changing moving paths is a continuum, which is actuated locally leading to a DoF of theoretically up to infinity. The more obvious biological paragon, which realizes this principle nearly perfectly, is obvious: the elephant's trunk. Structures like that are in meso and micro scale at present technologically not realizable. Biomimetics in its technical part for present customer demands must find at present technologically realizable solutions, biomimetics is no one way from biology to engineering. One first at present realizable step in the wanted direction for endo devices may the (phylogenetically back-) step from the structure of the vertebral column (which very roughly transferred underlies the present constructions) to that of its historical precursor *Chorda dorsalis* as a biomimetic paragon, as illustrated in Figure (2).

 doi:10.20944/preprints202402.0787.v1

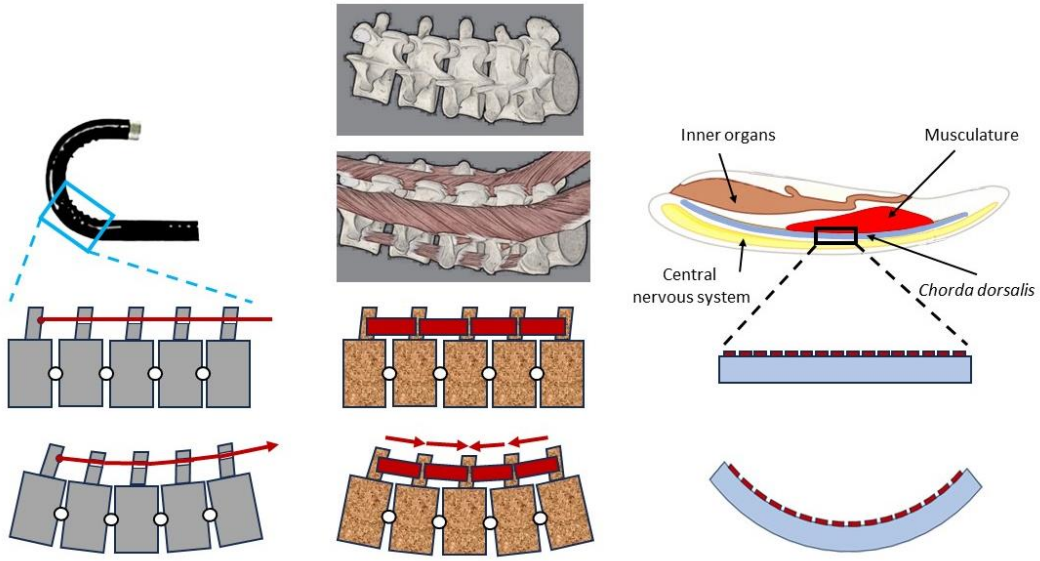

Figure 2. Left: principle of conventional endoscopes. Bending is realized by a series of rigid bodies (forming "segments"), rotating around defined joint axes. Motion of all segments is coupled by application of the same force via a Bowden drive. Center: principle of bending a vertebrates' spine. Comparable to the principle used in conventional endoscope, with the exception that rotation in all segments may be different, since forces are provided by intersegmental muscles. In the real animal, the rotation axis is slightly moving during motion, and additional longer muscles allow controlled coupled bending as well. Right: principle of Chorda dorsalis system in basic Chordates. The support structure is a compliant beam (in the natural paragon with changing geometry over length), which due to action of small muscles can be bent locally with different curvatures along the length. For reasons of clarity, motion is shown around one axis in one direction, in technology as in nature actuation in up to 3 rotational DoF in antagonistic manner may provide six overlaid rotational directions.

While the spine may be seen as a series of rigid segments, connected by "real" joints (diarthroses), actively moved by muscles bridging the gaps, Chorda dorsalis a continuous bending beam, to which local bending is imprinted by local muscle fibres. These allow the controlled application of bending moments and axial (compressive) forces. Transverse forces in a bending beam are coupled in a fixed manner to the bending moment around the transversal axis, thus they as well may be controlled in a coupled manner as 1 DoF.

The chorda is by no means a faulty construction, it has fulfilled its tasks for half a billion years and still fulfills them in recent animals. Beneath other factors, growing body masses and thus gravitational and inertial forces in combination with the utilization of torsional movements led to the evolution of the spinal column, which we as humans anthropocentrically consider to be the better solution. However, both the chorda and the spine are adapted to their respective tasks, and the chorda, with its lower load-bearing capacity but higher local bending, due to flexibility in combination with a monolithic structure when torsion is not required, corresponds better in its functional description to the requirements of an endoscope than a spine, so it is the more suitable biological paragon.

Derived from that (simplified) model of a chorda, we realized a demonstrator in meso scale with a, due to the lack of a yet not industrialized precise process at present feasible, very limited number of synergistic "muscle pairs" on a continuous flexible beam, which was formed by segments (technically: in modular design), which are rigidly coupled to resemble a monolithic structure.

 doi:10.20944/preprints202402.0787.v1

2.3. Proposed Soft Mechanism

Design, and Prototyping

Dominantly, soft pneumatic actuators contain silicon rubbers as their main material, and generally make use of a sort of asymmetry, either via asymmetric cross-section or strengthening fibers, to yield a directed motion when pressurized air is exerted. A McKibben actuator is a type of pneumatic muscle that is attractive for biomedical applications [21], with advantages of similarity with biological muscles, reliable safety, and good performance. The actuator consists of a hollow cylinder soft tube, and a braided reinforcing net [22]. A method of fabrication of small-size McKibben actuators was proposed in [23]. Using a braider machine, like the machines used for producing braided strings, as described in [24], the actuators are manufactured in long lengths that can be cut to desired size. In this study, we proposed a multi-segment McKibben-based soft probe, schematically shown in Figure 3.

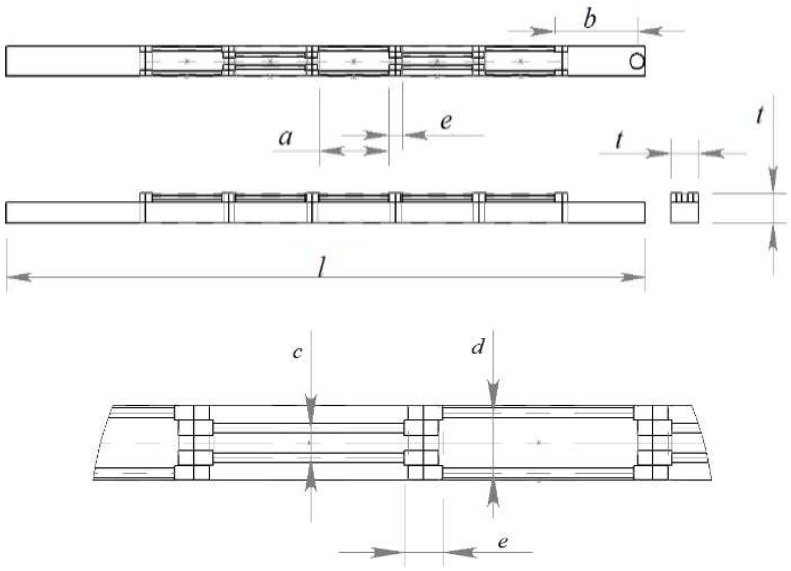

Figure 3. Design of the soft mechanism.

Each segment contains symmetrically to the midline two "muscles" or McKibben actuators of 1.3 mm diameter with equal lengths, a=25 mm. Table 1 represents the dimensions. Each actuator is connected to a pneumatic pressure source and controlled individually. To investigate feasibility of the proposed design, a prototype of the soft robot was fabricated. The main steps for prototyping are illustrated in Figure 4.

Table 1. Dimensions of the soft probe.

Parameter	Description	Amount (mm)
a	Length of actuators	25 ±1
b	Tip center position	27 ±0.1
c	Lateral distance	5±0.5
d	Lateral distance	8 ±0.5
e	Longitudinal distance	2 ±0.5
t	Core width	10 ±0.1

Preprints.org (www.preprints.org) | NOT PEER-REVIEWED | Posted: 14 February 2024 doi:10.20944/preprints202402.0787.v1

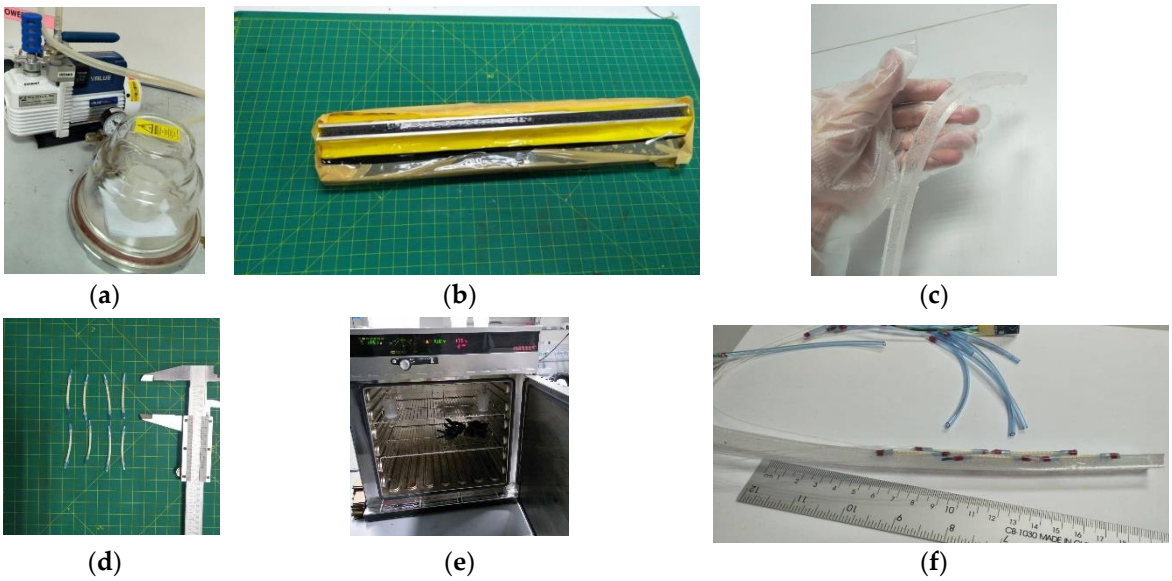

Figure 4. Prototyping the soft robot: (a) Vacuum of mixed material, (b) Molding, (c) Trimming, (d) Preparation of the muscles and pipes, (e) Adhesive curing, (f) The fabricated prototype.

For mechanical modelling purpose, we consider a single segment of the soft robot as in Figure 5. Due to compliance, the resistance force of the soft beam (bending stiffness) is negligible. This means that the external load on the McKibben actuators is zero, and their length depends on the pneumatic pressure. Thus, the quasi-static geometry relations and equations are represented as a function of the actuators' length.

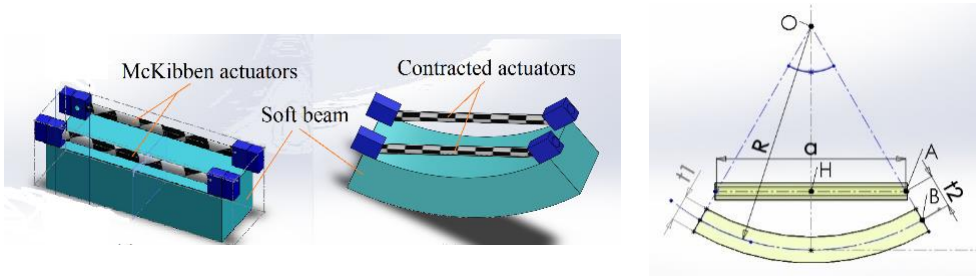

Figure 5. Schematic representation of segmental bending.

First, the material of the core was mixed and processed by a vacuum pump for approximately one hour to reduce bubbles. The material was cast in an aluminum mold. Then, the McKibben actuators were connected to 0.5 mm pipes, and attached to the core. For more robust attachment, the same mixture of the material was used as the adhesive and was cured in an oven. The electronic hardware for control of valves includes an Arduino® Mega and the interfacing circuits (using TBD62183AFNG) installed on the Arduino® as in Figure 6.

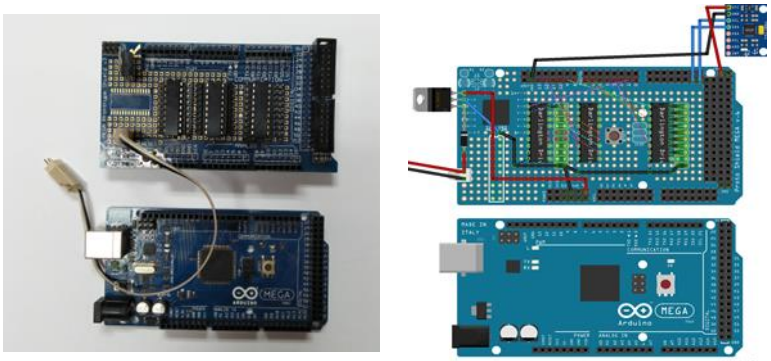

 doi:10.20944/preprints202402.0787.v1

Figure 6. The microcontroller system.

The pneumatic control system includes 10 miniature 3/2 NC Solenoid valves working with 24V. The actual system is shown in Figure 7.

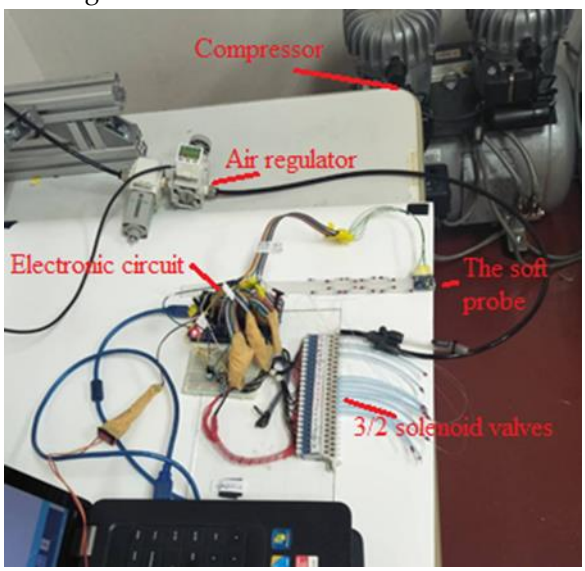

Figure 7. Final hardware setup.

The valve control system was programmed with MATLAB® and deployed on Arduino®. An MPU 6050 as the tilt sensor was added to system at the tip of the robot. It was programmed just to measure angles, though the sensor has more capabilities like acceleration measurement. The McKibben muscles can be pressurized individually.

Modelization

Suppose the actuator with initial length a_0 is contracted to $a < a_0$ result in the bending of the soft beam. Let be $\tau = t_1/2 + t_2$. Then for angle $\theta = \measuredangle AOH$ we have

$$a = 2(R-\tau)\mathrm{Sin}(\theta) \tag{5}$$

Defining contraction rate, $\lambda = a/a_0$, for the actuator is

$$a = 2\lambda\theta R \tag{6}$$

Combining (5) and (6) we get

$$2\tau\theta\,\mathrm{Sin}(\theta) + \lambda a_0\theta - a_0\,\mathrm{Sin}(\theta) = 0 \tag{7}$$

The nonlinear equation (7) can be solved for θ. An approximation can be written in series form as follows

$$\frac{2\tau}{5!}\theta^6 - \frac{a_0}{5!}\theta^5 - \frac{2\tau}{3!}\theta^4 + \frac{a_0}{3!}\theta^3 + 2\tau\theta^2 + (\lambda - a_0)\theta = 0 + O(\theta^7) \tag{8}$$

The length of the soft probe with three actuators is approximately equal to the TEE active part (and the two distal actuators are integrated for future use such as locomotion). For the three-segment model, the transformation matrix can be obtained by multiplying the transformation matrices of the segments, which in turn can be obtained in various ways. In this work, considering Figure 8, the coordinate system located at the tip is obtained by the following rotations and transformations of the base coordinate system. First, a rotation of θ_x around the current X axis, a transformation along the new X and Y axes to reach the tip point, O_1, and finally, a rotation of θ_z around the Z axis. In case the segment is not actuated, i.e., when the pressure is zero, the transformation matrix is given merely

 doi:10.20944/preprints202402.0787.v1

by a transformation along the X axis. The transformation matrix for segment 1 is represented by the double statement as follows.

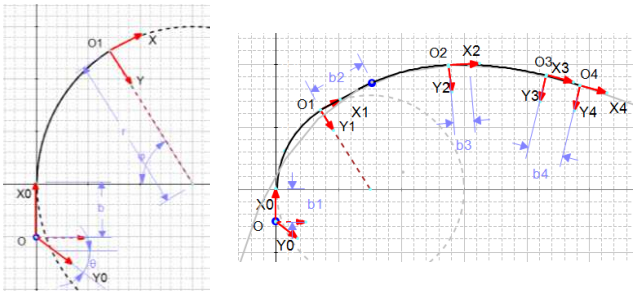

Figure 8. The coordinates and kinematic representation.

$$T_1 = \begin{cases} Rotx(\theta_{x1})Trans(b_1,0,0)* \\ \quad Trans(r_1.\sin(\theta_{z1}), r_1.[1-\cos(\theta_{z1})],0)Rotz(\theta_{z1}), \quad \text{(actuated)} \\ Trans(a_{01},0,0) \qquad \text{(not actuated)} \end{cases} \tag{9}$$

Similarly, for segments 2 and 3

$$T_2 = \begin{cases} Rotx(\theta_{x2})Trans(b_2,0,0)* \\ \quad Trans(r_2.\sin(\theta_{z2}), r_2.[1-\cos(\theta_{z2})],0)Rotz(\theta_{z2}), \\ Trans(a_{02},0,0) \end{cases} \tag{10}$$

$$T_3 = \begin{cases} Rotx(\theta_{x3})Trans(b_3,0,0)* \\ \quad Trans(r_3.\sin(\theta_{z3}), r_3.[1-\cos(\theta_{z3})],0)Rotz(\theta_{z3}), \\ Trans(a_{03},0,0) \end{cases} \tag{11}$$

Note that $a_{01} = a_{02} = a_{03} = a_0$ and $a_{0i} = r_i\theta_{zi}$. For the inactive part at the tip the transformation matrix is

$$T_4 = Trans(b,0,0) \tag{12}$$

Finally, with the homogeneous transformation matrix H, the tip position in frame $X_0Y_0Z_0$, denoted as $\vec{P}^0_{TipS}$, can be obtained related to its local coordinates as

$$H_{1\to4} = T_1T_2T_3T_4 \quad , \quad \vec{P}^0_{TipS} = H_{1\to4}\vec{P}^4_{Tip} \tag{13}$$

The application of actuators in pairs makes it possible to rotate the bending plate, and so the term *Rotx(.)* appeared based on the following description. When the actuators at both sides are equally contracted, the probe will show retroflex without lateral bending. However, if any pair of the adjacent actuators are operated with different pressures, the bending plate will rotate along X axis as shown in Figure 9.

Preprints.org (www.preprints.org) | NOT PEER-REVIEWED | Posted: 14 February 2024 doi:10.20944/preprints202402.0787.v1

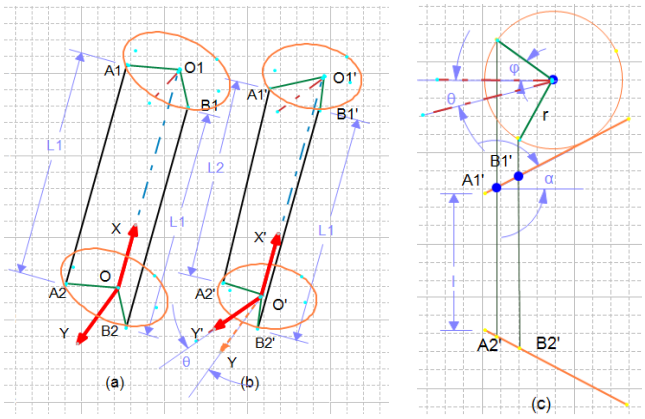

Figure 9. Rotation of the bending plate (a) equal contraction, (b) asymmetric bending, (c) The geometry.

As long as the length of actuators denoted as A_1A_2 and B_1B_2 are equal to L_1, the *Rotx(.)* term in the equations is zero. Otherwise,

$$L = l + 2\sin(\alpha).r.(1-\cos(\varphi)) \tag{14}$$

$$\begin{aligned} L_1 &= l + 2\sin(\alpha).r.(1-\cos(\varphi_1)) \\ L_2 &= l + 2\sin(\alpha).r.(1-\cos(\varphi_2)) \end{aligned} \tag{15}$$

$$L_1 - L_2 = 2\sin(\alpha).r.(\cos(\varphi_2) - \cos(\varphi_1)) \tag{16}$$

Then, the rotation angle is obtained as follows.

$$\theta_x = \theta = -0.5(\varphi_2 - \varphi_1) = -0.5\,\mathrm{Arccos}[(L_1 - L_2)/2\sin(\alpha).r] \tag{17}$$

The chosen state vector includes states of each segment that is the segmental bending angles. The soft probe is described with the following states

$$\begin{aligned} \vec{q}_S &= \left[\theta_{x1}, \theta_{z1}, \theta_{x2}, \theta_{z2}, \theta_{x3}, \theta_{z3}\right]^T \\ Q^{SoRo} &= \left\{\vec{q}_S \,\middle|\, 0 < \theta_{xi} < 20^o, 0 < \theta_{zi} < 50^o\right\} \end{aligned} \tag{18}$$

In comparison with the conventional probes, the soft robot has fundamental different structure and mechanics. While the conventional probe is a two DoF system with a 3D manifold workspace, the soft robot has six DoFs due to the six actuators on the active part. In fact, actuator redundancy is common in soft robots, but in most cases the actuators (*e.g.*, chambers in multi-chamber robots) share a single pressurizing tube. We investigate a method to make use of the redundancy to map the soft robot trajectory and workspace on those of the rigid counterpart. The next subsection explains the method.

Control Method

Neural Networks (NNs) are extensively used for the modelling and control of soft robots [25–27] to alleviate the complexity of mathematical modelling, making use of the advances in data science. However, the literature mainly deals with the modelling or control of soft robots as individual or independent devices like conventional robots. In this section, an algorithm is proposed to provide kinematic similarity between a reference system and a soft robot. We propose an NN based on the Kohonen (*aka* SOM) network and a nearest neighbour search (NNS), to provide the required kinematic similarity. The method is an unsupervised machine-learning technique that represents a two-dimensional map of the data set. Similar tools such as the k-means and related algorithms operate without topology preservation. The training is based on competitive learning. First, the distance of the input data W^R to all current weight vectors W^{SOM} is measured. Then, the neuron with

 doi:10.20944/preprints202402.0787.v1

the most similarity to the weight vector is labelled as the best matching unit (BMU). One single neuron is assigned as the *winning* neuron for the input points. Then, neighbour neurons in the grid are moved towards the input points. For any node j the number of data points, having the node as their BMU is calculated and assigned as, n_j. Then the weights are updated as a function of the average of the distances of the n_j points from the node j, denoted as $\bar{x}_j$ with the following rule

$$W^{SOM}\Big|_{node\ \ i} = \frac{\sum n_j h_{j,i} \bar{x}_j}{\sum n_j h_{j,i}} \tag{19}$$

Where, $h_{j,i}$ denotes a neighbourhood distance of winning node j to node i to spread the grid over the data set. The next task of the algorithm includes an NNS, which is a kind of proximity search. The points in the cloud of soft probe tip positions closest to the SOM nodes are labelled, and the corresponding states are recorded by the algorithm. The training algorithm, which contains the offline calculations, is given as Algorithm A (given in Appendix A) and is represented as the block diagram in Figure 10.

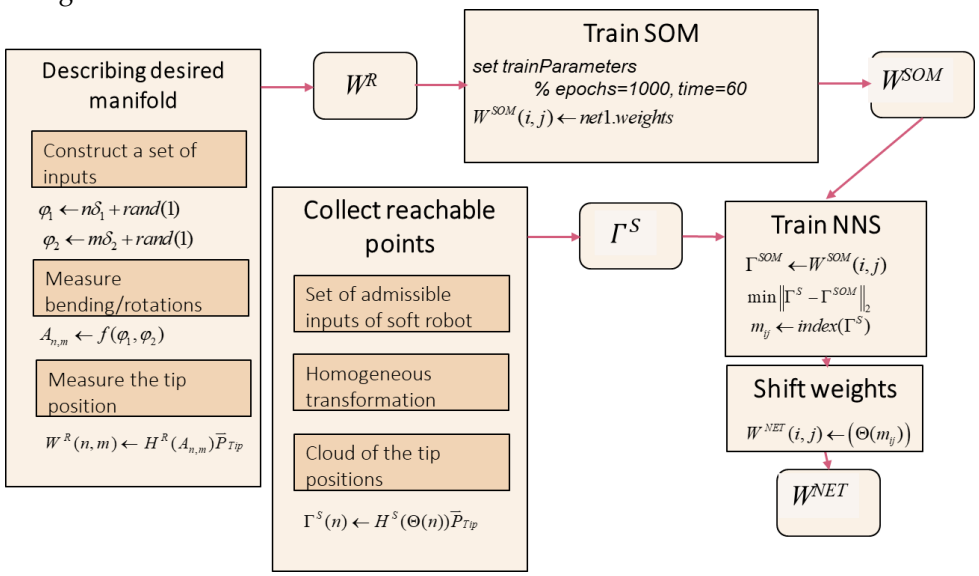

Figure 10. The training procedure.

In the training algorithm, φ_1, φ_2 can be seen as inputs of the reference system, $\delta_1 = (\varphi_1^{\max} - \varphi_1^{\min})/N$, $\delta_2 = (\varphi_2^{\max} - \varphi_2^{\min})/M$, and $N, M \in \mathbb{N}$. The set of admissible configuration angles is denoted as A. The subset $W^R \subset \mathbb{R}^3$ represents the workspace of the rigid system $|W^R| = NM$. The homogeneous transformation matrix is shown as H^R and the tip position vector in the relevant local coordinate system is Γ^R. The SOM network is constructed with a rectangular grid of size $N_{SOM} \times M_{SOM}$ and initial weights $W^{(PCA)}$. The trained SOM weight matrix is represented as W^{SOM}. For the soft robot, the state vector is represented as Θ, and the set of all admissible states is shown by B. The soft robot tip points are obtained with the soft robot transformation matrix H^S for all the n members of B.

For each $\Gamma^{SOM}(i,j) \in W^{SOM}$ and all $\Gamma^S(n)$, the index, m_{ij}, is found so that

$$\left\|\Gamma^S(m_{ij}) - \Gamma^{SOM}(i,j)\right\|_2 \le \left\|\Gamma^S(n) - \Gamma^{SOM}(i,j)\right\|_2 \tag{20}$$

Finally, the modified network weights are saved as W^{NET}. The NN maps the reference input to the follower input so that the outputs meet at the representative points. Algorithm A is used for constructing and training the NN. Algorithm B (given in Appendix B) represents the way the trained system is implemented for control.

 doi:10.20944/preprints202402.0787.v1

3. Results

The equations and relations given in the previous section were coded using MATLAB® to obtain numerical values of the tip position over all the conceivable gestures. Figure 11 shows the results for the soft and rigid probes. The cloud of points will be used to train or design the workspace. The graph shows necessarily the soft robot can localize the US sensor to any point that is reachable by the rigid probe. This is expected from the scale and geometric similarity, but there is no point-to-point relation between the sets. The dataset has a discrete and random nature, alternatively could collected from embodied systems, and the NN is the best tool to represent such data uniformly. In this stage, two questions arise: The first regarding the feasibility of practical fabrication of the soft robot, and the second regarding the method such system can be controlled. The next subsections deal with the investigation relevant to the questions.

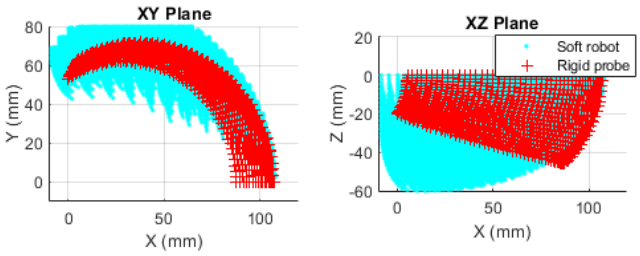

Figure 11. Representation of the tip access points for the soft robot and the rigid probe.

3.1. Fabrication and Testing

An experimental verification was used to evaluate the prototype as the demonstrator. For this purpose, the pneumatic circuit as shown in Figure 12 was used with an input signal that consequently (with 10 s intervals) opens the valves of each segment was considered. The test was performed for three contraction ratios a/L ($L=a_0$). The measured values are the tip angles. For a smooth transition, each pneumatic valve was excited with a PWM signal. However, only at the final states, the values were read. The results are summarized in Table II and Figure 13. A calibration may be used to make up for the errors. Nevertheless, the small errors in this work are ignored. Note that all the five segments were used in this test, so the transformation matrices of the other segments were included. Employing the standard pneumatic equipment enables us to make use of established pneumatics and commercially available components. In this work, miniature 3/2 solenoid valves with spring return were used. Proper excitation combination of the valves provides different gestures in the robot as in Figure 14. Nevertheless, to have control over the pressure, more complex proportional valves are suggested.

Preprints.org (www.preprints.org) | NOT PEER-REVIEWED | Posted: 14 February 2024 doi:10.20944/preprints202402.0787.v1

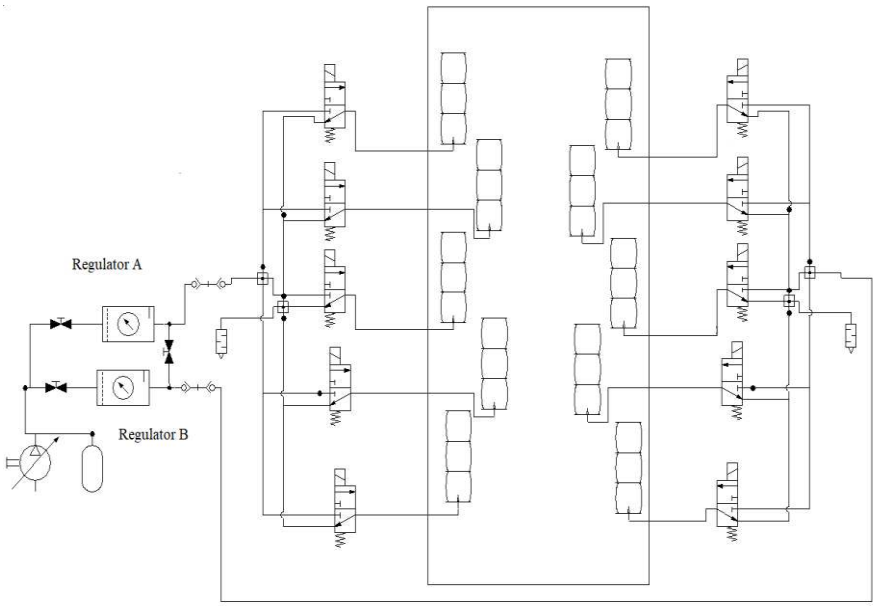

Figure 12. The pneumatic circuit.

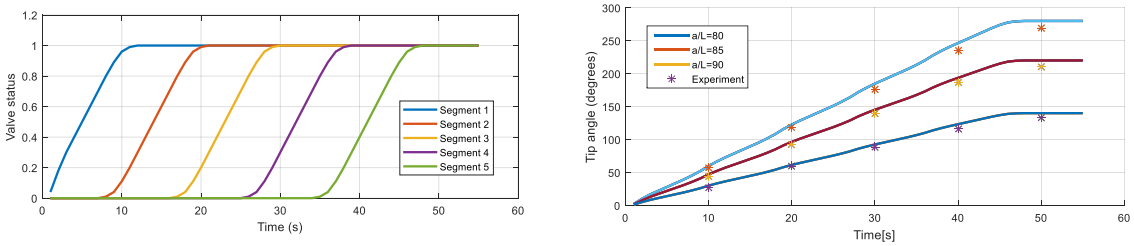

(**a**) (**b**)

Figure 13. Experiment of the prototype: (a) The input, (b) The response.

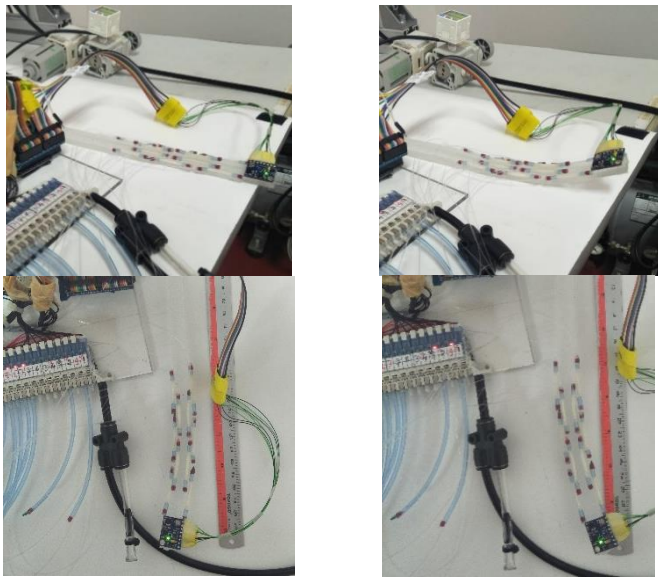

Figure 14. Bending to different directions.

Table 2. Numerical values.

a/a_0		Tip angle (°)				
80	Simulation	59.9	122.6	184.8	246.4	280

 doi:10.20944/preprints202402.0787.v1

	Experiment	57	118	176	235	269
	Error [1]	-4.8	-3.7	-4.8	-4.6	-3.9
85	Simulation	47.1	96.4	145.2	193.6	220
	Experiment	44	92	140	187	210
	Error	-6.6	-4.6	-3.6	-3.4	-4.5
90	Simulation	30	61.3	92.4	123.2	140
	Experiment	27	59	89	116	133
	Error	-10	-3.8	-3.7	-5.8	-5.0

[1]Error=(Experiment-Simulation)/Simulation*100.

3.2. Training Results and Error Analysis

Generally, success of training depends on many factors and need to be shown with experiments (*i.e.,* simulations). The result's numerical values have some randomness and can be different in different runs. Normally, repetition of training is required to achieve a good result. One advantage of the SOM nets is that the network has some visual presentation that can be used to observe the results. If the training result is not sufficiently good, some nodes will appear outside of the data (the desired manifold in this work), or the nodes do not spread uniformly. In that case, the training can be repeated by refining the parameters. The trained network used in this work is represented in Figure 15. The neurons are represented as a square lattice as in Figure 15 (a), where the nodes represent neurons that are loaded with weights shown in Figure 15 (b). The result of NNS is shown in Figure 15 (c). In feedforward neural networks, an error number is calculated that can be used to indicate the training result. However, in the unsupervised NN, the error cannot be calculated by normal means. In fact, unsupervised learning has not defined error because there is no ideal data to calculate the error against it. Many SOM implementations do not even report an error and the literature does not provide an error calculation method. The worst distance from BMUs may be taken as the error, but such an index is used in the algorithm to stop the training when the learning is not improved more. In this work, the distance between the tip of the soft robot with that of the rigid probe model is considered as the error.

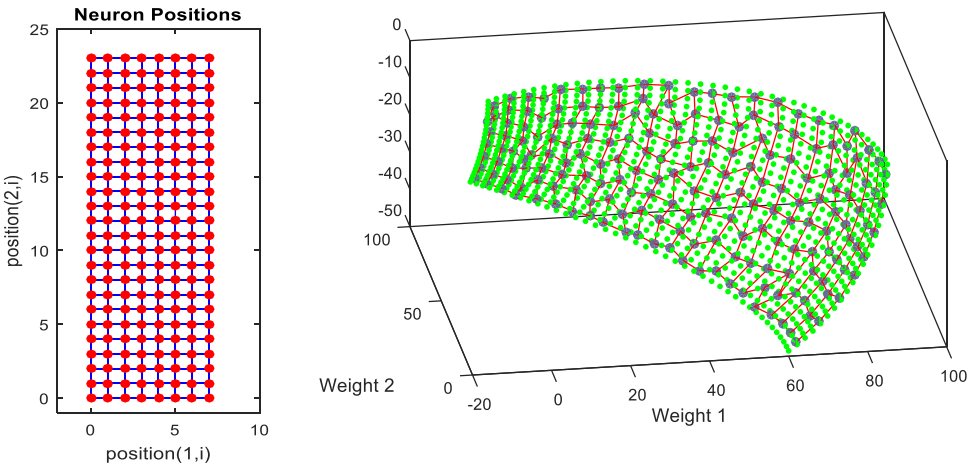

(**a**) (**b**)

Preprints.org (www.preprints.org) | NOT PEER-REVIEWED | Posted: 14 February 2024 doi:10.20944/preprints202402.0787.v1

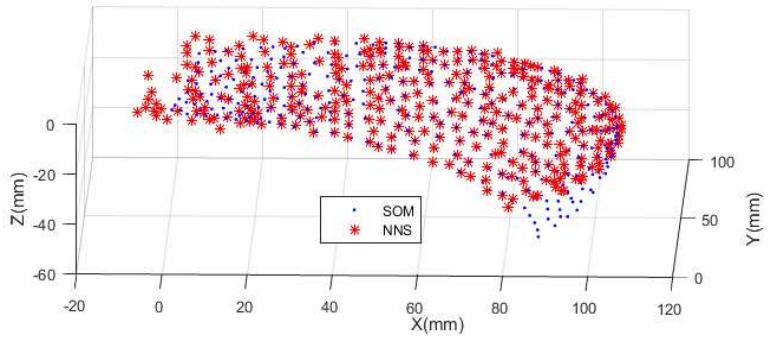

(c)

Figure 15. Topology of the trained network: (a) Lattice of neurons, (b) The SOM weights, (c) NNS nodes vs. the SOM weights.

The error may be examined over the whole workspace. The NN algorithm was used to map the representative points of the workspace of the rigid probe, to the workspace of the controlled soft robot (as in Figure 16). The error was calculated by moving average represented in Figure 17, using MATLAB® syntax:

avErr = tsmovavg(sqrt(e),'s',15,2);

minimumDist =0.143 mm

maximumDist =18.0 mm

RMSE =4.36 mm

The *RMSE* value over the whole workspace is less than 5 mm. However, the maximum value shows a large error. The error can be reduced, for example, by increasing the resolution of the NN or the number of neurons, which in turn increases the size of weight matrices, complexity, and calculation time (and delay). However, the large errors appear mainly at the ends of the workspace where the probe is either close to the straight initial status or bent to maximum angles. These states are not important as they have no contribution to US imaging.

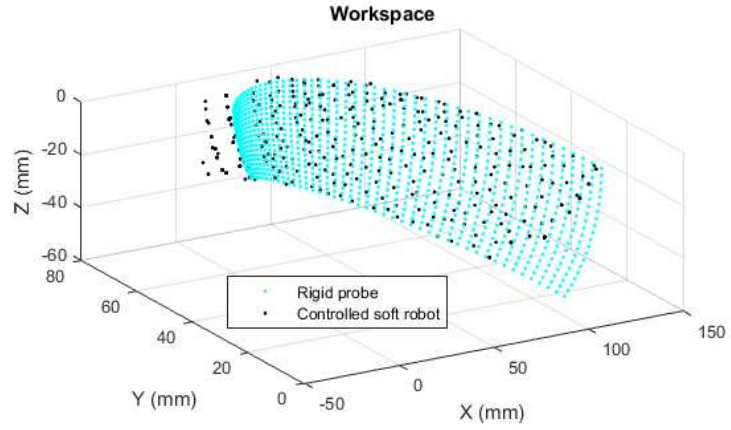

Figure 16. Comparison on the workspace.

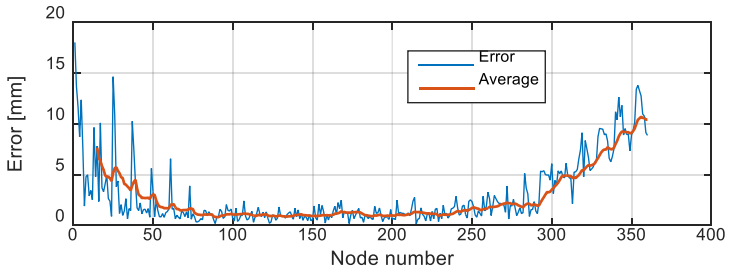

Figure 17. The corresponding error.

 doi:10.20944/preprints202402.0787.v1

3.3. Case-Study Simulations

To examine the method in the trajectory following scenarios, two simulations are presented as case studies. In Figure 18, the desired trajectories are shown by the red line on the reference workspace manifold. The stars represent the weight of excited neurons, and the robot's path is shown by the black line. The errors are shown in Figure 19 consequently. (Note that the examples presented here are essentially arbitrary, but we had some clues from medical experts regarding practical scenarios and the normalized flexing and bending during the scenarios were reconstructed as Figure 20 and used in the simulation.)

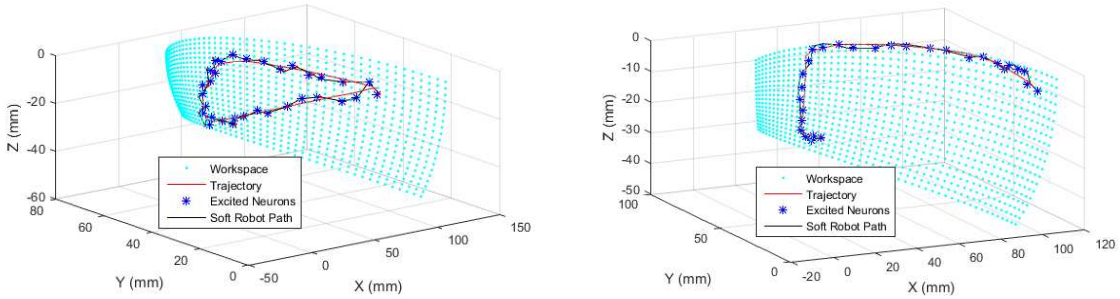

Figure 18. The simulation results.

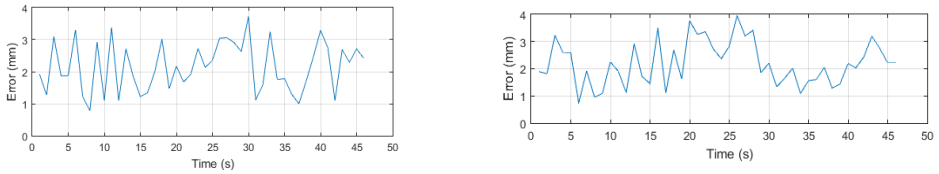

Figure 19. The trajectory errors.

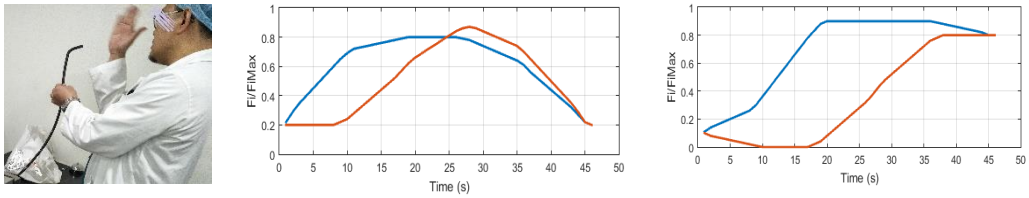

Figure 20. Description of the example scenarios.

4. Discussion

Soft mechanisms, due to their inherent compliance, are prospective candidates for development of the next-generation ultrasound imaging probes. In comparison to conventional robotics, soft robotics relies more on empirical investigations. To assimilate soft robots within the medical context, further developments are required in addition to a pure robotics study that is not confined by such medical requirements. In this work, we proposed a soft robot based on McKibben actuators that work with standard ranges of industrial pneumatic pressures (up to 600 kPa). The robot was made with equipment, components, and materials commonly accessible in academic soft robotics laboratories that have experience with soft pneumatic systems. A prototype was made to demonstrate the feasibility of fabrication and evaluate the kinematic performance. Next, the medical requirement or constraint dealt with in this study was retaining a kinematic similarity with the conventional system as the reference. This goal is partly achieved by designing the robot with the scale of the distal end of the probe. Additionally, the tip of the soft robot where the US sensor is placed, should have access to all the points reachable by that of the traditional system (As discussed by comparison of the workspaces). In particular, point-to-point access to the workspace corresponding to the conventional system is necessary. Note that in a TEE scenario, the sonographer first adjusts the location of the US sensor at the tip of the probe using the knobs, based on their experience, and then tune adjustment

 doi:10.20944/preprints202402.0787.v1

of the US image is done electronically. A resolution of mechanical motion (within the range of 5 mm, according to our medical advisors) should be considered over the workspace. By the resolution, we mean the distance between the tip of the soft robot with the desired position. It is denoted as resolution (not error) because the proposed algorithm can be retrained with different numbers of neurons to achieve different resolutions. If higher numbers of neurons are used, the resolution can be finer at the expense of the complexity of the control system. Basically, SOMs mimic the self-organizing capabilities observed in the brain's neural networks. The network can be trained with experimental data as well, and continuity of the soft robot input is not necessary. The results show the capability of the system to satisfy the requirements and make the method recommendable for similar applications. The medical probes used in US imaging are not moved fast and so can be described by quasi-static models, and with a kinematic matching, a soft robot will behave like the rigid counterpart without needing excessive training for the sonographer. Last but not least, the soft robot, even when actuated, is compliant with respect to external forces. This is in contrast to the cable-driven probes which become rigid when they are bent and can cause serious injuries by crashing the patient's tissues.

5. Conclusions

In this research, a soft robotic solution was developed for TEE as the medical application. The proposed solution includes a physical soft probe as well as an NN-based control algorithm for open-loop maneuvering. The first soft robot uses McKibben artificial muscles that work with positive pressures. The quasi-static models were derived and verified by some experiments. The models consist of the kinematic equations relating the segmental curvatures, considered as the state vector, to the tip position. The relation between the input pressure to the curvature in the segments is obtained by experimental calibration. The concept of similarity requirement was introduced in this study. The proposed kinematic matching technique provides a similarity between probe tip positions with targeted deviations (less than 5 mm), in terms of maximum distance in two typical paths, and more generally, in terms of RMSE over the workspace. The results convince us that the soft robot can replicate the TEE probe and have advantages in terms of safety and usability.

Author Contributions: Conceptualization, M.S. and H.W.; methodology, M.S.; software, M.S.; validation, M.S. and A.F.; formal analysis, M.S.; investigation, M.S. and H.W.; resources, A.F. and H.W.; data curation, M.S.; writing—original draft preparation, M.S. and A.F.; writing—review and editing, H.W. and M.S.; visualization, M.S. and H.W.; supervision, A.F. and H.W.; project administration, H.W.; funding acquisition, A.F. and H.W. All authors have read and agreed to the published version of the manuscript.

Funding: This study was partially supported by the Thuringian State Graduate Support. We acknowledge support for the publication costs by the Open Access Publication Fund of Technische Universität Ilmenau.

Institutional Review Board Statement: Not applicable.

Data Availability Statement: Data sharing is not applicable to this article.

Acknowledgments: The authors would like to express inclusive thanks to the Institut Jantung Negara (IJN), National Heart Institute, Malaysia; for permitting observation and measurements of TEE probes and their consultations.

Conflicts of Interest: The authors declare no conflict of interest.

 doi:10.20944/preprints202402.0787.v1

Appendix A

Algorithm A: Training

Initialization
For n=1 to N
  $\varphi_1 \leftarrow n\delta_1 + rand(1)$
  For m=1 to M
    $\varphi_2 \leftarrow m\delta_2 + rand(1)$
    $A_{n,m} \leftarrow f(\varphi_1, \varphi_2)$
    $W^R(n,m) \leftarrow H^R(A_{n,m})\vec{P}_{Tip}$
Set $N_{SOM} = 12, M_{SOM} = 30$
net1=selforgmap(NSOM, MSOM)
epochs=1000, time=60 % Set training parameters
net1 $\leftarrow$ *train(net1,epochs,time)* % Start training of *net1*
$W^{SOM}(i,j) \leftarrow net1.weights$ % Save the results in the weight matrix
Load(B) % Load the set of admissible bending angles
For n in $\Theta(n) \in B$
  $\Gamma^S(n) \leftarrow H^S(\Theta(n))\vec{P}_{Tip}$

For i=1:N_{SOM}
  For j=1:M_{SOM}
    $\Gamma^{SOM} \leftarrow W^{SOM}(i,j)$
    $\min \left\| \Gamma^S - \Gamma^{SOM} \right\|_2$ % For query point Γ^{SOM} find Γ^S
    $m_{ij} \leftarrow index(\Gamma^S)$

For i=1:N_{SOM}
  For j=1:M_{SOM}
    $W^{NET}(i,j) \leftarrow \left(\Theta(m_{ij})\right)$

end

Appendix B

Algorithm B: Controller

Initialization
  While loop
    $(\varphi_1, \varphi_2) \leftarrow (\varphi_1, \varphi_2)^{desired}$ % Read the inputs
    $A_{1,2} \leftarrow f(\varphi_1, \varphi_2)$
    $\Gamma^R \leftarrow H^R(A_{1,2})\vec{P}_{Tip}$
    $(i,j) = index(network(\Gamma^R))$
    $\Theta \leftarrow W^{NET}(i,j)$
    $delay(\Delta t)$ % Next time step
end

References

1. Sayahkarajy, M. Mode shape analysis, modal linearization, and control of an elastic two-link manipulator based on the normal modes. *Applied Mathematical Modelling* **2018**, *59*, 546-570.
2. Andrada, E.; Mämpel, J.; Schmidt, A.; Fischer, M.; Karguth, A.; Witte, H. From biomechanics of rats'inclined locomotion to a climbing robot. *International Journal of Design Nature Ecodynamics* **2013**, *8*, 192-212.
3. Zhong, Y.; Hu, L.; Xu, Y. Recent advances in design and actuation of continuum robots for medical applications. In Proceedings of the Actuators, 2020; p. 142.
4. Sayahkarajy, M.; Witte, H. Soft medical robots and probes: Concise survey of current advances. *Design, Construction, Maintenance* **2023**, *3*, 263-278, doi:10.37394/232022.2023.3.26.

5. Kondoyanni, M.; Loukatos, D.; Maraveas, C.; Drosos, C.; Arvanitis, K.G. Bio-Inspired robots and structures toward fostering the modernization of agriculture. *Biomimetics* **2022**, *7*, 69.
6. Hahn, R.T.; Abraham, T.; Adams, M.S.; Bruce, C.J.; Glas, K.E.; Lang, R.M.; Reeves, S.T.; Shanewise, J.S.; Siu, S.C.; Stewart, W. Guidelines for performing a comprehensive transesophageal echocardiographic examination: recommendations from the American Society of Echocardiography and the Society of Cardiovascular Anesthesiologists. *Journal of the American Society of Echocardiography* **2013**, *26*, 921-964.
7. Zhang, H.; Wang, J.; Guo, C. Tool frame calibration for robot-assisted ultrasonic testing. *Sensors* **2023**, *23*, 8820.
8. Hidalgo, E.M.; Wright, L.; Isaksson, M.; Lambert, G.; Marwick, T.H. Current applications of robot-assisted ultrasound examination. *Cardiovascular Imaging* **2023**, *16*, 239-247.
9. Wang, S.; Housden, J.; Bai, T.; Liu, H.; Back, J.; Singh, D.; Rhode, K.; Hou, Z.-G.; Wang, F.-Y. Robotic intra-operative ultrasound: virtual environments and parallel systems. *IEEE/CAA Journal of Automatica Sinica* **2021**, *8*, 1095-1106.
10. Xie, Y.; Hou, X.; Wang, S. Design of a novel haptic joystick for the teleoperation of continuum-mechanism-based medical robots. *Robotics* **2023**, *12*, 52.
11. Sayahkarajy, M.; Mohd Faudzi, A. A. Design of a mechatronic interface with compliant manipulator for robot assisted echocardiography. In Proceedings of the Journal of Physics, Conference Series, 2021; p. 012005.
12. Witte, H. The interplay of biomimetics and biomechatronics. *Biomimetics* **2022**, *7*, 96.
13. Stano, G.; Percoco, G. Additive manufacturing aimed to soft robots fabrication: A review. *Extreme Mechanics Letters* **2021**, *42*, 101079.
14. Lee, C.; Kim, M.; Kim, Y.J.; Hong, N.; Ryu, S.; Kim, H.J.; Kim, S. Soft robot review. *International Journal of Control, Automation and Systems* **2017**, *15*, 3-15.
15. Faudzi, A.A.; Azmi, N.I.; Sayahkarajy, M.; Xuan, W.L.; Suzumori, K. Soft manipulator using thin McKibben actuator. In Proceedings of the 2018 IEEE/ASME International Conference on Advanced Intelligent Mechatronics (AIM), 2018; pp. 334-339.
16. Conrad, S.; Teichmann, J.; Auth, P.; Knorr, N.; Ulrich, K.; Bellin, D.; Speck, T.; Tauber, F. 3D-printed digital pneumatic logic for the control of soft robotic actuators. *Science Robotics* **2024**, *9*, eadh4060.
17. Duanmu, D.; Li, X.; Huang, W.; Hu, Y. Soft finger rehabilitation exoskeleton of biomimetic dragonfly abdominal ventral muscles: Center tendon pneumatic bellows actuator. *Biomimetics* **2023**, *8*, 614.
18. Banerjee, H.; Tse, Z.T.H.; Ren, H. Soft robotics with compliance and adaptation for biomedical applications and forthcoming challenges. *International Journal of Robotics and Automation* **2018**, *33*.
19. Zhang, Y.; Lu, M. A review of recent advancements in soft and flexible robots for medical applications. *The International Journal of Computer Assisted Radiology and Surgery* **2020**, *16*, e2096.
20. Junghanns, H. Der Lumbosakralwinkel: Messungen an Röntgenbildern und frischen Präparaten. *Deutsche Zeitschrift für Chirurgie* **1929**, *213*, 322-340.
21. Xiang, C.; Guo, J.; Chen, Y.; Hao, L.; Davis, S. Development of a SMA-fishing-line-McKibben bending actuator. *IEEE Access* **2018**, *6*, 27183-27189.
22. Daerden, F.; Lefeber, D. Pneumatic artificial muscles: actuators for robotics and automation. *European Journal of Mechanical and Environmental Engineering* **2002**, *47*, 11-21.
23. De Volder, M.; Moers, A.; Reynaerts, D. Fabrication and control of miniature McKibben actuators. *Sensors and Actuators A: Physical* **2011**, *166*, 111-116.
24. Tian, W.; Wakimoto, S.; Yamaguchi, D.; Kanda, T. Fabrication process for twisting artificial muscles by utilizing braiding technology and water-soluble fibers. *IEEE Robotics Automation Letters* **2024**.
25. Salem, M.E.; Wang, Q.; Xu, M.H. Application of neural network fitting for modeling the pneumatic networks bending soft actuator behavior. *Engineering Research Express* **2022**.
26. Kim, D.; Kim, S.-H.; Kim, T.; Kang, B.B.; Lee, M.; Park, W.; Ku, S.; Kim, D.; Kwon, J.; Lee, H. Review of machine learning methods in soft robotics. *Plos one* **2021**, *16*, e0246102.
27. Li, Y.; Cao, Y.; Jia, F. A neural network based dynamic control method for soft pneumatic actuator with symmetrical chambers. In Proceedings of the Actuators, 2021; p. 112.